

Through the Dual-Prism: A Spectral Perspective on Graph Data Augmentation for Graph Classifications

Yutong Xia^{1*}, Runpeng Yu^{1*}, Yuxuan Liang^{2†},
Xavier Bresson¹, Xinchao Wang^{1†}, Roger Zimmermann¹

¹National University of Singapore

²The Hong Kong University of Science and Technology (Guangzhou)

{yutong.xia,r.yu}@u.nus.edu; yuxliang@outlook.com; {xaviercs,xinchao,dcsr}@nus.edu.sg

Abstract

Graph Neural Networks have become the preferred tool to process graph data, with their efficacy being boosted through graph data augmentation techniques. Despite the evolution of augmentation methods, issues like graph property distortions and restricted structural changes persist. This leads to the question: *Is it possible to develop more property-conserving and structure-sensitive augmentation methods?* Through a spectral lens, we investigate the interplay between graph properties, their augmentation, and their spectral behavior, and observe that keeping the low-frequency eigenvalues unchanged can preserve the critical properties at a large scale when generating augmented graphs. These observations inform our introduction of the Dual-Prism (DP) augmentation methods, including DP-Noise and DP-Mask, which retain essential graph properties while diversifying augmented graphs. Extensive experiments validate the efficiency of our approach, providing a new and promising direction for graph data augmentation.

Code — <https://github.com/ru-yu/DualPrism>

Introduction

Graph structures, modeling complex systems through nodes and edges, are ubiquitous across various domains, including social networks (Newman, Watts, and Strogatz 2002), bioinformatics (Yi et al. 2022), and transportation systems (Jin et al. 2023a). Graph Neural Networks (GNNs) (Kipf and Welling 2016a) elegantly handle this relational information for tasks like accurate predictions. Their capabilities are further enhanced by graph data augmentation techniques, which artificially diversify the dataset via strategic manipulations, thereby improving the performance and generalization of GNNs. Graph data augmentation has progressed from early random topological modifications, e.g. DropEdge (Rong et al. 2019) and DropNode (Feng et al. 2020), to sophisticated learning-centric approaches like InfoMin (Suresh et al. 2021). Furthermore, techniques inspired by image augmentation’s mixup principle (Zhang et al. 2017) have emerged as prominent contenders (Verma et al. 2019; Wang et al. 2021; Guo and Mao 2021).

Though promising, these augmentation methods are challenged by three key issues as follows. (1) *Graph Property Distortion*. Before the era of deep learning, graph properties, e.g., graph connectivity and diameter, served as vital features for classification for decades (Childs et al. 2009). While now they seem to be ignored, many aforementioned contemporary augmentation methods appear to sidestep this tradition and overlook the graph properties. For instance, an example graph from the IMDB-BINARY dataset (Morris et al. 2020) and its augmented graph via DropEdge are illustrated in Figures 1a and 1b, respectively. The polar plot in Figure 1e shows the properties of these graphs, where each axis represents a distinct property. It is evident that DropEdge significantly alters the original graph’s properties, as indicated by the stark difference between the shapes of the orange (original) and blue (augmented) pentagons. (2) *Limited Structural Impact*. The majority of existing methods’ localized alterations do not capture the broader relationships and structures within the graph, limiting their utility. Consider a social network graph, where removing an edge affects just the immediate node and does little to alter the overall community structure. We thus ask: Can we design more *property-retentive* and *structure-aware* data augmentation techniques for GNNs?

Through the Dual-Prism: A Spectral Lens. Graph data augmentation involves altering components of an original graph. These modifications, in turn, lead to changes in the graph’s spectral frequencies (Ortega et al. 2018). Recent research highlighted the importance of the graph spectrum: it can reveal critical graph properties, e.g., connectivity and radius (Chung 1997; Lee, Gharan, and Trevisan 2014). Additionally, it also provides a holistic summary of a graph’s intrinsic structure (Chang et al. 2021), providing a global view for graph topology alterations. Building on this foundation, a pivotal question arises: *Could the spectral domain be the stage for structure-aware and property-retentive augmentation efforts?* Drawing inspiration from *dual prisms*—which filter and reconstruct light based on spectral elements—can we design a *polarizer* to shed new light on this challenge? With this in mind, we use spectral graph theory, aiming to answer the following questions: 1) Can a spectral approach to graph data augmentation preserve essential graph properties effectively? 2) How does spectral-based augmentation impact broader graph structures? 3) How does spectral-

Copyright © 2025, Association for the Advancement of Artificial Intelligence (www.aaai.org). All rights reserved.

* Y. Xia and R. Yu contributed equally to this work.

† Y. Liang and X. Wang are the corresponding authors.

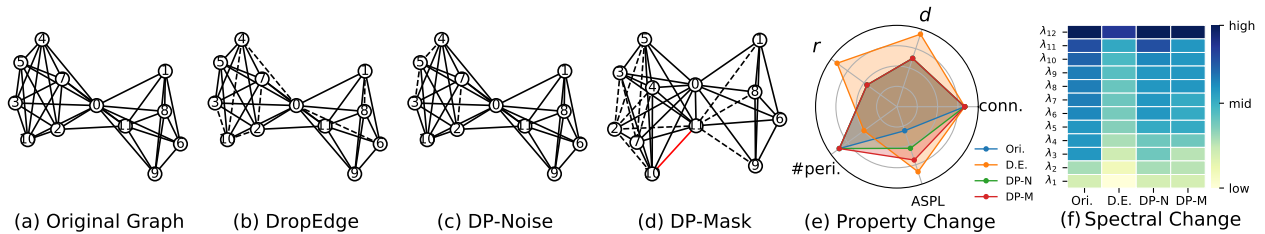


Figure 1: Visualization of (a) a graph from the IMDB-BINARY dataset and its augmented graphs via (b) DropEdge (Rong et al. 2019), (c) DP-Noise (ours), and (d) DP-Mask (ours). Dashed line: Dropped edge. Red line: Added edge. (e) Five properties of these graphs. r : radius. d : diameter. conn.: connectivity. ASPL: average shortest path length. #peri: number of periphery. Ori.: Original. D.E.: DropEdge. DP-N: DP-Noise. DP-M: DP-Mask. (f) The eigenvalues of these four graphs.

based augmentation compare to existing methods in enhancing the efficiency of GNNs for graph classification?

We begin with an empirical exploration, where we aim to understand the interplay between topological modifications and their spectral responses. Our insights reveal that changes in graph properties mainly manifest in *low-frequency components*. Armed with this, we unveil our Dual-Prism (DP) augmentation strategies, DP-Noise and DP-Mask, by only changing the high-frequency part of the spectrum of graphs. Figures 1c and 1d provide a visualization of the augmented graphs via our proposed methods, i.e., DP-Noise and DP-Mask. As shown in Figure 1e, compared with DropEdge, our approaches skillfully maintain the inherent properties of the original graph, differing only slightly in the ASPL. Note that although we solely present one example underscoring our method’s capability, its robustness is consistently evident across all scenarios.

In addition to the properties, we further explore the spectrum comparison, shown in Figure 1f. Compared with DropEdge, the spectrum shifts caused by our methods are noticeably smaller. Interestingly, despite our approaches’ relative stability in the spectral domain, they induce substantial changes in the spatial realm (i.e., notable edge modifications). This spectral stability helps retain the core properties, while the spatial variations ensure a rich diversity in augmented graphs. Conversely, DropEdge, despite only causing certain edge changes, disrupts the spectrum and essential graph properties significantly. Simply put, **our methods skillfully maintain graph properties while also diversifying augmented graphs**. In the Experiments section, we evaluate the efficacy of our methods on graph classification, across diverse settings: supervised, semi-supervised, unsupervised, and transfer learning on various real-world datasets. Our concluding thoughts are presented in the last section.

Contributions. Our main contributions are outlined as follows. (1) *Prism – Bridging Spatial and Spectral Domains*: We introduce a spectral lens to shed light on spatial graph data augmentation, aiming to better understand the spectral behavior of graph modifications and their interplay with inherent graph properties. (2) *Polarizer – Innovative Augmentation Method*: We propose the globally-aware and property-retentive augmentation methods, Dual-Prism (DP), including DP-Noise and DP-Mask. Our methods are able to preserve inherent graph properties while si-

multaneously enhancing the diversity of augmented graphs. (3) *New Light – Extensive Evaluations*: We conduct comprehensive experiments spanning supervised, semi-supervised, unsupervised, and transfer learning paradigms on 21 real-world datasets. The experimental results demonstrate that our proposed methods can achieve state-of-art performance on the majority of datasets.

Related Work

Data Augmentations for GNNs. Graph data augmentation refers to the process of modifying a graph to enhance or diversify the information contained within, which can be used to bolster the training dataset for better generalization or model variations in real-world networks (Ding et al. 2022; Zhao et al. 2022). Early methods are grounded in random modification to the graph topology. Techniques like DropEdge (Rong et al. 2019), DropNode (Feng et al. 2020), and random subgraph sampling (You et al. 2020) introduce stochastic perturbations in the graph structure. In addition to random modification, there is a wave of methods utilizing more sophisticated, learning-based strategies to generate augmented graphs (Suresh et al. 2021). Another research line is inspired by the efficiency of mixup (Zhang et al. 2017) in image augmentation, blending node features or entire subgraphs to create hybrid graph structures (Verma et al. 2019; Wang et al. 2021; Guo and Mao 2021; Han et al. 2022; Park, Shim, and Yang 2022; Ling et al. 2023). However, while the above techniques have advanced the field of graph data augmentation, challenges remain, especially in preserving broader structural changes and graph semantics.

Spectrum and GNNs. Spectral graph theory (Chung 1997) has significantly influenced GNNs (Ortega et al. 2018; Wu et al. 2019; Dong et al. 2020; Bo et al. 2021; Chang et al. 2021; Yang et al. 2022), evolving from defining early GNN convolutions using the Laplacian spectrum (Hammond, Vandergheynst, and Gribonval 2011; Defferrard, Bresson, and Vandergheynst 2016) to enhancing scalability (Nt and Maehara 2019). This approach is pivotal in various domains, including graph contrastive learning (GCL) (Liu et al. 2022; Lin, Chen, and Wang 2022; Yang et al. 2023; Chen, Lei, and Wei 2024), adversarial attacks (Entezari et al. 2020; Chang et al. 2021), and multivariate time series (Cao et al. 2020; Jin et al. 2023b). Zooming into the GCL domain, where data augmentation plays a pivotal role, (Liu et al. 2022) introduced the general rule of effective augmented graphs

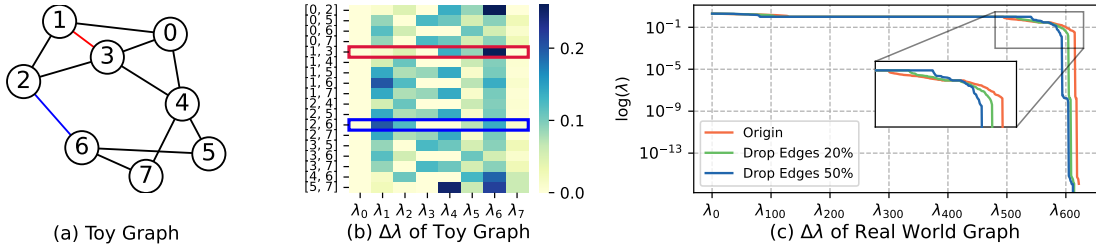


Figure 2: (a) A toy graph \mathcal{G} consisting of eight nodes. (b) Absolute variation in eigenvalues of \mathcal{G} when adding an edge at diverse positions. The red and blue rectangles represent when adding the corresponding edges in \mathcal{G} and the change of the eigenvalues. (c) A real-world case in the REDDIT-BINARY dataset where, when dropping 20% and 50%, the high frequency is more vulnerable.

in GCL via a spectral perspective; GCL-SPAN (Lin, Chen, and Wang 2022) presented a novel augmentation method for GCL, focusing on the invariance of graph representation in the spectral domain; GASSER (Yang et al. 2023) uses a selective perturbation across various frequency bands to maintain homophily ratios while introducing perturbations to optimize task-relevant features; and PolyGCL (Chen, Lei, and Wei 2024) demonstrates the spectral filters can be effectively utilized for contrastive learning on graphs. Though promising, these methods do not fully address the intricacies of maintaining *inherent graph properties* during augmentation.

A Spectral Lens on Graph Data Augmentations

Preliminaries. An undirected graph \mathcal{G} is represented as $\mathcal{G} = (V, E)$ where V is the set of nodes with $|V| = N$ and $E \subseteq V \times V$ is the set of edges. Let $A \in \mathbb{R}^{N \times N}$ be the adjacency matrix of \mathcal{G} , with elements $a_{ij} = 1$ if there is an edge between nodes i and j , and $a_{ij} = 0$ otherwise. Let $D \in \mathbb{R}^{N \times N}$ be the degree matrix, which is a diagonal matrix with elements $d_{ii} = \sum_j a_{ij}$, representing the degree of node i . The Laplacian matrix of \mathcal{G} is denoted as $L = D - A \in \mathbb{R}^{N \times N}$. The eigen-decomposition of L is denoted as $U\Lambda U^T$, where $\Lambda = \text{diag}(\lambda_1, \dots, \lambda_N)$ and $U = [u_1^T, \dots, u_N^T] \in \mathbb{R}^{N \times N}$. For graph \mathcal{G} , L has n non-negative real eigenvalues $0 \leq \lambda_1 \leq \lambda_2 \leq \dots \leq \lambda_N$. Specifically, the *low-frequency components* refer to the eigenvalues closer to 0, and the *high-frequency components* refer to the relatively larger eigenvalues.

Spectral Analysis Insights

Adopting a spectral viewpoint, we conduct a thorough empirical study to understand the interplay between graph properties, graph topology alterations in the spatial domain, and their corresponding impacts in the spectral domain. The findings from our analysis include four crucial aspects as detailed below.

Obs 1. The position of the edge flip influences the magnitude of spectral changes. In Figures 2a and 2b, we explore how adding different edges to a toy graph affects its eigenvalues. For instance, the addition of the edge $1 \leftrightarrow 3$ (shown as the red line), which connects two proximate nodes, primarily impacts the high-frequency component λ_6 (the red rectangle). In contrast, when adding edge $2 \leftrightarrow 6$ (the

blue line) between two distant nodes, the low-frequency component λ_1 exhibits the most noticeable change (the blue rectangle). These variations in the spectrum underscore the significance of the edge-flipping position within the graph’s overall topology, whose insight is consistent with findings by (Entezari et al. 2020; Chang et al. 2021). Such spectral changes not only affect the graph’s inherent structural features but also potentially affect the outcomes of tasks relying on spectral properties, such as graph-based learning.

Obs 2. Low-frequency components display greater resilience to edge alterations. Building on Obs 1, we further investigate the different responses of high- and low-frequency components to topology alterations using a real-world graph. We apply DropEdge (Rong et al. 2019) for augmentation by first randomly dropping 20% and 50% of edges and then computing the corresponding eigenvalues, as depicted in Figure 2c. It can be observed that, under random edge removal, low-frequency components exhibit greater robustness compared to their high-frequency counterparts.

Obs 3. Graph properties are crucial for graph classification. Certain fundamental properties of graphs, e.g., diameter and radius, are critical for a variety of downstream tasks, including graph classification (Feragen et al. 2013). In Figures 4a and 4b, we present the distributions of two key graph properties – diameter d and radius r – across the two classes in the REDD-M12 dataset. The different variations in these distributions emphasize their critical role in graph classification. Nevertheless, arbitrary modifications to the graph’s topology, e.g., random-manner-based augmentation techniques, could potentially distort these vital properties, illustrated in Figures 1b and 1e.

Obs 4. Specific low-frequency eigenvalues are closely tied to crucial graph properties. From Obs 3, a question is raised: *Can we retain the integrity of these essential graph properties during augmentation?* To explore this, we turn our attention back to the toy graph in Figure 2a and examine the evolution of its properties and eigenvalues in response to single-edge flips. In Figures 4c and 4d, we chart the graph’s average shortest path length (denoted by blue dots), diameter d (denoted by green dots) against the reciprocal of its second smallest eigenvalue $1/\lambda_1$ (denoted by red dots)*. Our observations reveal a notable correlation between the alterations in d and $1/\lambda_1$.

*For visual clarity, we scaled d and $1/\lambda_1$ by dividing it by 3 and 5, respectively.

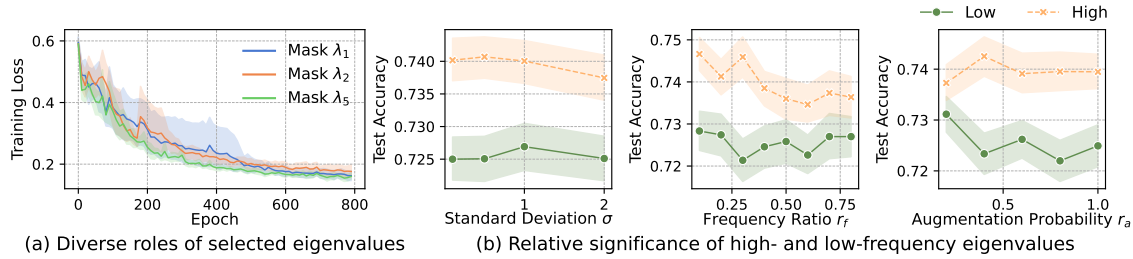


Figure 3: (a) Training loss of GIN model on REDDIT-BINARY when graphs are augmented by masking different eigenvalues. (b) Graph classification performance on IMDB-BINARY under various hyperparameters. The lines represent the average accuracy, while the shaded areas indicate the error margins.

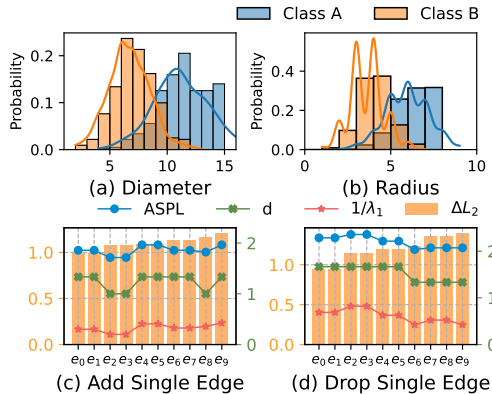


Figure 4: (a) Diameter and (b) radius distributions of different classes in REDD-M12. When (c) adding or (d) removing an edge, variation of the spectral domain ΔL_2 , $1/\lambda_1$ of \mathcal{G}' , ASPL and diameter d of \mathcal{G}' .

Further, we investigate correlations among overall spectral shifts, graph properties, and specific eigenvalues. Consistent with established methodologies (Lin, Chen, and Wang 2022; Wang et al. 2022; Wills and Meyer 2020), we adopt the Frobenius distance to quantify the overall spectral variations by computing the L_2 distance between the spectrum of \mathcal{G} and augmented graph \mathcal{G}' . Notably, this spectral shift does not directly correspond with the changes in properties or eigenvalues. This suggests that by maintaining critical eigenvalues, primarily the low-frequency components, we can inject relatively large spectral changes without affecting essential graph properties. This observation thus leads to our proposition: *preserving key eigenvalues while modifying others enables the generation of augmented graphs that uphold foundational properties*, instead of only focusing on the overall spectral shifts.

Methodology

Drawing inspiration from how prisms decompose and reconstruct light and how a polarizer selectively filters light (Figure 5a), we design our own “polarizer”, i.e., the **Dual-Prism** (DP) method for graph data augmentation (Figure 5b).

Proposed Augmentation Methods

The proposed DP methods, including *DP-Noise* and *DP-Mask*, obtain the augmented graphs by directly changing

the spectrum of graphs. A step-by-step breakdown is delineated in Algorithm 1. The DP method starts by extracting the Laplacian Matrix L of a graph \mathcal{G} by $L = D - A$ and then computes its eigen-decomposition $L = U\Lambda U^T$. Based on the frequency ratio r_f , N_a eigenvalues are selected for augmentation, where $N_a = N \times r_f$. Note that since we only target high-frequency eigenvalues, we arrange eigenvalues in increasing order and only focus on the *last* N_a eigenvalues. Then, a binary mask M is formed based on the augmentation ratio r_a to sample the eigenvalues to make a change. Depending on the chosen augmentation type T , either noise is infused to the sampled eigenvalues, modulated by σ and M (from Line 6 to 8), or the eigenvalues are adjusted using the mask M directly (from Line 9 to 10). Finally, we reconstruct the new Laplacian \hat{L} based on the updated eigenvalues $\hat{\Lambda}$. Given the Laplacian matrix is $L = D - A$, where D is a diagonal matrix, an updated adjacency matrix \hat{A} can be derived by eliminating self-loops. Lastly, we obtain the augmented graph $\hat{\mathcal{G}}$ with its original labels and features retained. **Selection of L .** Note that we adopt the Laplacian matrix L instead of the normalized Laplacian matrix $L_{\text{norm}} = I - D^{-1/2}AD^{-1/2}$. The rationale behind this choice is that reconstructing the adjacency matrix using L_{norm} necessitates solving a system quadratic equation, where the number of unknown parameters equals the number of nodes in the graph. The computational complexity of this solution is more than $O(N^3)$. Even if we approximate it as a quadratic optimization problem, making it solvable with a gradient-based optimizer, the computational overhead introduced by solving such an optimization problem for each graph to be augmented is prohibitively high.

Empirical Evidence

Next, we verify our methods on the improvement of the performance for graph classification via experimental analysis. **Diverse roles of eigenvalues.** We begin by masking selected eigenvalues to generate graphs for 20% of REDDIT-BINARY. The training loss when masking the eigenvalues λ_1 , λ_2 and λ_5 is shown in Figure 3a. These curves suggest that individual eigenvalues contribute differently to the training process. Specifically, masking λ_1 results in a notably unstable training loss for the initial 500 epochs, evidenced by the expansive blue-shaded region. For λ_2 , while the shaded region’s extent is smaller, the curve exhibits noticeable fluctuation.

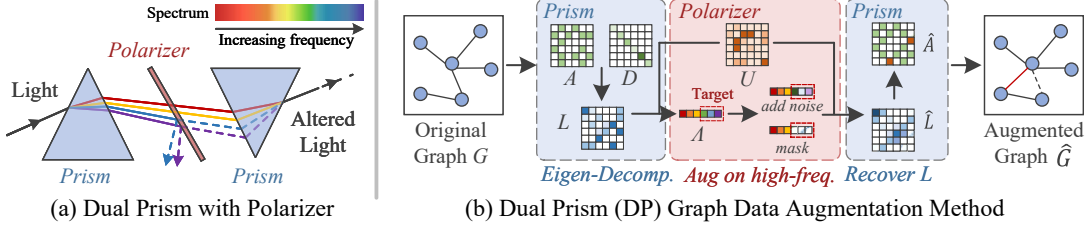


Figure 5: The framework of our Dual-Prism (DP) for graph data augmentation.

tuations, particularly around epoch 200. Conversely, when masking λ_5 , the training appears more stable, with the green curve showing relative steadiness and a reduced shaded area. These demonstrate the various significance of eigenvalues: λ_1 and λ_2 include more crucial structural and property details of the graph compared to λ_5 . As a result, they deserve to be prioritized for preservation during augmentation.

Different importance of high- and low-frequency parts.

We then conduct experiments on group-level eigenvalues, i.e., the high- and low-frequency ones, to gain a broader view of the influence exerted by varying frequency eigenvalues. We introduce noise to eigenvalues across various hyperparameter combinations. Concretely, we use the standard deviation σ to determine the magnitude of the noise. The frequency ratio r_f dictates the number of eigenvalues N_a we might change, while the augmentation probability r_a specifies the final eigenvalues sampled for modification. The eigenvalues are arranged in ascending order. The setting of 'Low' means that we select candidates from the first N_a eigenvalues, while 'High' denotes selection from the last N_a eigenvalues. As shown in Figure 3b, the orange lines consistently outperform the green lines across all three plots, indicating that the performance associated with perturbing high-frequency eigenvalues consistently exceeds that of their low-

frequency counterparts. Moreover, as the frequency ratio r_f increases, the accuracy of the 'Low' scenario remains relatively stable and low. Contrastingly, for the 'High' scenario, a notable decline in accuracy begins once the ratio exceeds around 30%. This suggests that the eigenvalues outside the top 30% of the high-frequency range may start to include more critical information beneficial for graph classification tasks that should not be distorted.

Theoretical Backing and Insights

The eigenvalues of the Laplacian matrix provide significant insights into various graph properties (Chung 1997). Such insights have driven and backed our proposal to modify the high-frequency eigenvalues while preserving their low-frequency counterparts. For example, the second-smallest eigenvalue λ_1 , often termed the *Fiedler value*, quantifies the graph's *algebraic connectivity*. A greater Fiedler value indicates a better-connected graph and it is greater than 0 if and only if the graph is connected. The number of times 0 appears as an eigenvalue is the number of connected components in the graph. In addition to the connectivity, the diameter of a graph is also highly related to the eigenvalues – it can be upper and lower bounded from its spectrum (Chung 1997): $4/n\lambda_1 \leq d \leq 2[\sqrt{2m/\lambda_1} \log_2 n]$, where n and m denotes the number of nodes and the maximum degree of the graph. Besides these widely-used ones, other properties are also highly related to spectrum, e.g., graph diffusion distance (Hammond, Gur, and Johnson 2013). In essence, eigenvalues serve as powerful spectral signatures comprising a myriad of structural and functional aspects of graphs.

Experiments

Experimental Setup. We evaluate our method for graph classification under four different settings, including supervised learning, semi-supervised learning, unsupervised learning, and transfer learning. We conduct our experiments on 21 real-world datasets across three different domains, including bio-informatics, molecule, and social network, from the TUDatasets (Morris et al. 2020), OGB (Hu et al. 2020a) and ZINC chemical molecule dataset (Hu et al. 2020b).

Supervised Learning

Performance. We first evaluate our proposed methods in the supervised learning setting. Following the prior works (Han et al. 2022; Ling et al. 2023), we use GIN and GCN as backbones for graph classification on eight different datasets. Table 1 shows the performance of DP methods compared

Algorithm 1: Dual-Prism Augmentation

Input: Graph \mathcal{G} , Frequency Ratio r_f , Augmentation Ratio r_a , Standard Deviation σ , Augmentation Type T .

- 1: $N \leftarrow$ the number of nodes in \mathcal{G}
- 2: $L \leftarrow$ Laplacian Matrix of \mathcal{G}
Λ is arranged in increasing order.
- 3: U and $\Lambda \leftarrow$ eigenvalue decomposition of L
Get the number of eigenvalues to be augmented.
- 4: $N_a \leftarrow \text{int}(N \times r_f)$
- 5: $M \leftarrow \{m_i \sim \text{Bern}(r_a)\}_{i=1}^{N_a}$
Add noise to the high-frequency part.
- 6: **if** $T = \text{noise}$ **then**
- 7: $\epsilon \leftarrow \{\epsilon_i \sim \mathcal{N}(0, 1)\}_{i=1}^{N_a}$
- 8: **for** $i \in \{1, \dots, N_a\}$ **do** $\{\lambda_{N-i} \leftarrow \max(0, \lambda_{N-i} + \sigma M_i \epsilon_i)\}$
Mask the high-frequency part.
- 9: **else if** $T = \text{mask}$ **then**
- 10: **for** $i \in \{1, \dots, N_a\}$ **do** $\{\lambda_{N-i} \leftarrow (1 - M_i)\lambda_i\}$
Calculate the new Laplacian and new adjacent matrix.
- 11: $\hat{L} \leftarrow U^\top \hat{\Lambda} U, \hat{A} \leftarrow -\hat{L}$
- 12: **for** $i \in \{1, \dots, N\}$ **do** $\{\hat{A}_{ii} \leftarrow 0\}$

Output: Augmented $\hat{\mathcal{G}}$ with edge_index derived from \hat{A} , and the label and features unchanged

	Dataset	IMDB-B	IMDB-M	REDD-B	REDD-M5	REDD-M12	PROTEINS	NC11	ogbg-molhiv
GCN	Vanilla	72.80±4.08	49.47±2.60	84.85±2.42	49.99±1.37	46.90±0.73	71.43±2.60	72.38±1.45	96.80±0.06
	DropEdge	73.20±5.62	49.00±2.94	85.15±2.81	51.19±1.74	47.08±0.55	71.61±4.28	68.32±1.60	96.53±0.07
	DropNode	73.80±5.71	50.00±4.85	83.65±3.63	47.71±1.75	47.93±0.64	72.69±3.55	70.73±2.02	96.52±0.14
	Subgraph	70.90±5.07	49.80±3.43	68.41±2.57	47.31±5.23	47.49±0.93	67.93±3.24	65.05±4.36	96.49±0.17
	M-Mixup	72.00±5.66	49.73±2.67	<u>87.05±2.47</u>	51.49±2.00	46.92±1.05	71.16±2.87	71.58±1.79	-
	SubMix	72.30±4.75	49.73±2.88	85.15±2.37	52.87±2.19	-	72.42±2.43	71.65±1.58	-
	G-Mixup	73.20±5.60	50.33±3.67	86.85±2.30	51.77±1.42	<u>48.06±0.53</u>	70.18±2.44	70.75±1.72	-
	S-Mixup	74.40±5.44	50.73±3.66	89.30±2.69	53.29±1.97	-	73.05±2.81	75.47±1.49	96.70±0.20
	DP-Noise	77.90±2.30 *	53.60±1.59 **	84.60±7.61	53.42±1.36	48.47±0.57	75.03±2.66	69.20±2.57	97.02±0.19 **
	DP-Mask	76.00±3.62	51.20±1.73	76.70±1.34	52.42±2.78	47.25±1.12	73.60±3.10	62.45±3.80	96.90±0.24 *
GIN	Vanilla	71.30±4.36	48.80±2.54	89.15±2.47	53.17±2.26	50.23±0.83	68.28±2.47	79.08±2.12	96.54±0.11
	DropEdge	70.50±3.80	48.73±4.08	87.45±3.91	54.11±1.94	49.77±0.76	68.01±3.22	76.47±2.34	96.48±0.09
	DropNode	72.00±6.97	45.67±2.59	88.60±2.52	53.97±2.11	49.95±1.70	69.64±2.98	74.60±2.12	96.51±0.16
	Subgraph	70.40±4.98	43.74±5.74	76.80±3.87	50.09±4.94	49.67±0.90	66.67±3.10	60.17±2.33	96.49±0.13
	M-Mixup	72.00±5.14	48.67±5.32	87.70±2.50	52.85±1.03	49.81±0.80	68.65±3.76	79.85±1.88	-
	SubMix	71.70±6.20	49.80±4.01	90.45±1.93	54.27±2.92	-	69.54±3.15	79.78±1.09	-
	G-Mixup	72.40±5.64	49.93±2.82	90.20±2.84	54.33±1.99	<u>50.50±0.41</u>	64.69±3.60	78.20±1.58	-
	S-Mixup	73.40±6.26	50.13±4.34	90.55±2.11	55.19±1.99	-	69.37±2.86	80.02±2.45	96.84±0.40
	DP-Noise	78.40±1.82 **	61.67±0.71 **	93.42±1.41 **	57.72±1.87 **	53.70±1.16 **	73.51±4.54 **	90.56±5.78 **	97.43±0.48 **
	DP-Mask	76.30±2.56	51.60±1.32	93.25±1.19**	56.50±0.80*	49.11±1.30	72.79±1.95**	80.30±2.01	96.98±0.29

Table 1: Performance comparisons with GCN and GIN in the *supervised* learning setting. The best and second best results are highlighted with **bold** and underline, respectively. * and ** denote the improvement over the second best baseline is statistically significant at level 0.1 and 0.05 (Newey and West 1987). Baseline results are taken from (Ling et al. 2023; Han et al. 2022).

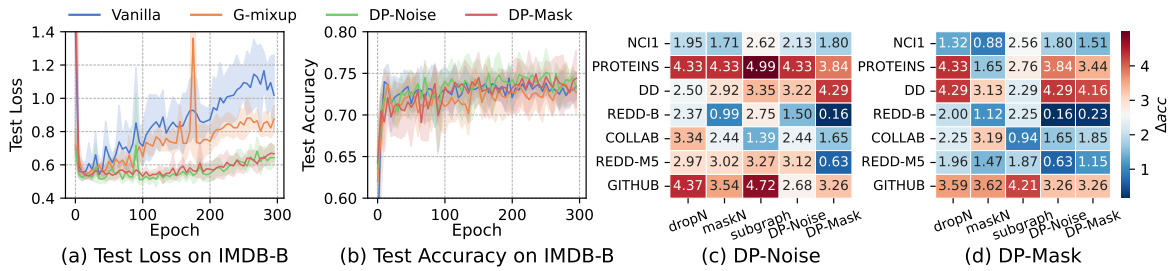


Figure 6: (a) The loss and (b) accuracy curves for supervised learning on test data of IMDB-BINARY using GIN, with four augmentation methods. Curves represent mean values from 5 runs, and shaded areas indicate standard deviation. The accuracy gain (%) in semi-supervised learning when contrasting 5 different augmentation methods with (c) DP-Noise and (b) DP-Mask across 7 datasets. Warmer color means better performance gains.

Dataset	NC11	COLLAB	GITHUB
Vallina	60.72±0.45	57.46±0.25	54.25±0.22
Aug.	60.49±0.46	58.40±0.97	56.36±0.42
GAE	61.63±0.84	63.20±0.67	59.44±0.44
Infomax	62.72±0.65	61.70±0.77	58.99±0.50
GraphCL	62.55±0.86	64.57±1.15	58.56±0.59
DP-Noise	63.43±1.39	65.94±3.13	60.06±2.72
DP-Mask	62.43±1.08	<u>65.68±1.66</u> *	59.70±0.53

Table 2: Performance comparisons in the *semi-supervised* learning setting with 1% label ratio. The best and second best results are highlighted with **bold** and underline, respectively. Baseline results are taken from (You et al. 2020).

with seven state-of-art (SOTA) baselines, including DropEdge(Rong et al. 2019), DropNode(Feng et al. 2020), Subgraph(You et al. 2020), M-Mixup(Verma et al. 2019), SubMix(Yoo, Shim, and Kang 2022), G-Mixup(Han et al. 2022) and S-Mixup(Ling et al. 2023). According to the results, DP-Noise consistently outperforms other existing methods across the majority of datasets, establishing its dominance in effectiveness. DP-Mask also shines, often securing a second-place standing. GIN tends to obtain superior outcomes, especially when combined with DP-Noise, exemplified by its

61.67% accuracy on IMDB-M. Note that on REDD-B, GIN achieves more satisfactory performance than GCN, which is a consistent pattern across baselines but becomes particularly pronounced with our methods. This phenomenon may be attributed to the intrinsic characteristics of GIN and GCN: GIN is known for its precision in capturing the complex structures of graphs (Xu et al. 2018), while GCN is characterized by its smoothing effect (Defferrard, Bresson, and Vandergheynst 2016). Our methods’ superiority in diversifying the graphs’ structures naturally amplifies GIN’s strengths. In contrast, GCN may not be as adept at leveraging the enhancements offered by our techniques.

Generalization. Figures 6a and 6b display the test loss and accuracy curves for the IMDB-B dataset, comparing four distinct augmentation strategies: G-mixup, DP-Noise, DP-Mask, and a scenario without any augmentation (i.e., Vanilla). The consistently lower and more stable test loss curves for DP-Noise and DP-Mask is comparison to Vanilla and G-mixup. Concurrently, the accuracy achieved with DP-Noise and DP-Mask is higher, indicating the DP methods’ superior generalization and the capacity for enhancing model stability.

Dataset	NCII	PROTEINS	DD	COLLAB	REDD-B	REDD-M5	GITHUB
Vallina	73.72±0.24	70.40±1.54	73.56±0.41	73.71±0.27	86.63±0.27	51.33±0.44	60.87±0.17
Aug.	73.59±0.32	70.29±0.64	74.30±0.81	74.19±0.13	87.74±0.39	52.01±0.20	60.91±0.32
GAE	74.36±0.24	70.51±0.17	74.54±0.68	75.09±0.19	87.69±0.40	<u>53.58±0.13</u>	63.89±0.52
Infomax	74.86±0.26	72.27±0.40	75.78±0.34	73.76±0.29	88.66±0.95	53.61±0.31	65.21±0.88
GraphCL	74.63±0.25	74.17±0.34	76.17±1.37	74.23±0.21	89.11±0.19	52.55±0.45	65.81±0.79
DP-Noise	75.30±0.58**	74.73±1.01	76.91±0.81	77.05±0.82**	89.38±0.95	54.45±0.64**	65.59±0.88
DP-Mask	74.88±1.84	71.37±4.18	75.64±0.81	76.90±0.62**	88.62±0.63	52.80±0.59	64.95±1.03

Table 3: Performance comparisons in the *semi-supervised* learning setting with 10% label ratio. The best and second best results are highlighted with **bold** and underline, respectively. The metric is accuracy (%). * and ** denote the improvement over the second-best baseline is statistically significant at levels 0.1 and 0.05. Baseline results are taken from (You et al. 2020).

Dataset	NCII	PROTEINS	DD	MUTAG	REDD-B	REDD-M5	IMDB-B
sub2vec	52.84±1.47	53.03±5.55	-	61.05±15.80	71.48±0.41	36.68±0.42	55.26±1.54
graph2vec	73.22±1.81	73.30±2.05	-	83.15±9.25	75.78±1.03	47.86±0.26	71.10±0.54
InfoGraph	76.20±1.06	74.44±0.31	75.23±0.39	89.01±1.13	82.50±1.42	53.46±1.03	73.03±0.87
GraphCL	77.87±0.41	74.39±0.45	<u>78.62±0.40</u>	86.80±1.34	89.53±0.84	55.99±0.28	71.14±0.44
MVGRL	68.68±0.42	74.02±0.32	75.20±0.55	89.24±1.31	81.20±0.69	51.87±0.65	71.84±0.78
AD-GCL	69.67±0.51	73.59±0.65	74.49±0.52	89.25±1.45	85.52±0.79	53.00±0.82	71.57±1.01
JOAO	72.99±0.75	71.25±0.85	66.91±1.75	85.20±1.64	78.35±1.38	45.57±2.86	71.60±0.86
GCL-SPAN	71.43±0.49	75.78±0.41	75.78±0.52	89.12±0.76	83.62±0.64	54.10±0.49	73.65±0.69
DP-Noise	79.69±0.70	74.60±0.43	78.59±0.23	87.63±1.98	<u>90.90±0.32**</u>	55.54±0.15	71.42±0.41
DP-Mask	79.47±0.22	74.70±0.29	79.97±1.09**	89.98±1.36	91.21±0.24**	55.92±0.49	71.78±0.37

Table 4: Performance comparisons in the *unsupervised* learning results. The best and second best results are highlighted with **bold** and underline. The metric is accuracy (%). * and ** denote the improvement over the second-best baseline is statistically significant at levels 0.1 and 0.05, respectively. Baseline results are taken from (You et al. 2020; Lin, Chen, and Wang 2022).

Semi-supervised Learning

Performance. We then evaluate our methods in a semi-supervised setting comparing with five baselines, including training from scratch without and with augmentations (denoted as Vanilla and Aug.), GAE (Kipf and Welling 2016b), Informax (Veličković et al. 2018) and GraphCL(You et al. 2020). Tables 2 and 3 provide the performance comparison when utilizing 1% and 10% label ratios. At the more challenging 1% label ratio, DP-Noise achieves SOTA results across all three datasets, and DP-Mask secures the second-best performance on two out of the three datasets. As the label ratio increases to 10%, DP-Noise maintains its efficacy, showing SOTA performance on six out of seven datasets.

Augmentation Pairing Efficiency. To investigate optimal combinations that could potentially enhance performance, we evaluate the synergistic effects on accuracy gain (%) when pairing DP-Noise and DP-Mask with different augmentation methods using the same setting in (You et al. 2020). From Figures 6c and 6d, overall, the diverse accuracy gains across datasets indicate that there is no one-size-fits-all “partner” for DP-Noise and DP-Mask; the efficacy of each combination varies depending on the dataset. However, generally, both DP-Noise and DP-Mask exhibit enhanced performance when paired with dropN at a large degree.

Unsupervised Representation Learning

We next evaluate DP methods in unsupervised learning and compare them with eight baselines, including three representation learning methods (sub2vec(Adhikari et al. 2018), graph2vec(Narayanan et al. 2017) and InfoGraph(Sun et al. 2019)) and five GCL-based methods (GraphCL(You et al. 2020), MVGRL(Hassani and Khasahmadi 2020), AD-GCL(Suresh et al. 2021), JOAO(You et al. 2021) and GCL-SPAN(Lin, Chen, and Wang 2022)). Table 4 shows the performance of our methods in an unsupervised setting. From

the results, DP methods surpass other baselines on five out of seven datasets. Notably, compared with another spectral-based method GCL-SPAN (Lin, Chen, and Wang 2022), our methods outperform it on most datasets, especially on the molecules dataset NCII (an increase of around 11.5% accuracy). This superiority can be attributed to the fact that while GCL-SPAN is also spectral-based, it operates on graph modification in the spatial domain rather than directly manipulating the spectral domain like DP methods. Given the critical role that structural patterns in molecular data play on classification tasks, the enhanced performance underscores the efficiency of our direct spectral modifications in creating more effective and insightful augmented graphs.

Transfer Learning

We conduct transfer learning experiments on molecular property prediction in the manner of (Hu et al. 2020b). Specifically, we initially pre-train models on the extensive chemical molecule dataset ZINC (Sterling and Irwin 2015), then fine-tune the models on eight distinct datasets within a similar domain. Due to space constraints, the table containing performance comparisons and analysis is provided in the Appendix.

Conclusion

In this study, we adopt a spectral perspective, bridging graph properties and spectral insights for property-retentive and globally-aware graph data augmentation. Stemming from this point, we propose a novel augmentation method DP, including DP-Noise and DP-Mask. By focusing on different frequency components in the spectrum, our method skillfully preserves graph properties while ensuring diversity in augmented graphs. Our extensive experiments validate the efficacy of our methods across various learning paradigms on the graph classification task.

Acknowledgements

This work is partially supported by the Advanced Research and Technology Innovation Centre (ARTIC), the National University of Singapore under Grant (project number: ELDT-RP2), and by National Research Foundation, Singapore, under its AI Singapore Programme (AISG Award No: AISG2-RP-2021-023). It is also supported by the National Natural Science Foundation of China (No. 62402414). Xavier Bresson is supported by NUS Grant ID R-252-000-B97-133.

References

- Adhikari, B.; Zhang, Y.; Ramakrishnan, N.; and Prakash, B. A. 2018. Sub2vec: Feature learning for subgraphs. In *Advances in Knowledge Discovery and Data Mining: 22nd Pacific-Asia Conference, PAKDD 2018, Melbourne, VIC, Australia, June 3-6, 2018, Proceedings, Part II 22*, 170–182. Springer.
- Bo, D.; Wang, X.; Shi, C.; and Shen, H. 2021. Beyond low-frequency information in graph convolutional networks. In *Proceedings of the AAAI Conference on Artificial Intelligence*, volume 35, 3950–3957.
- Cao, D.; Wang, Y.; Duan, J.; Zhang, C.; Zhu, X.; Huang, C.; Tong, Y.; Xu, B.; Bai, J.; Tong, J.; et al. 2020. Spectral temporal graph neural network for multivariate time-series forecasting. *Advances in neural information processing systems*, 33: 17766–17778.
- Chang, H.; Rong, Y.; Xu, T.; Bian, Y.; Zhou, S.; Wang, X.; Huang, J.; and Zhu, W. 2021. Not all low-pass filters are robust in graph convolutional networks. *Advances in Neural Information Processing Systems*, 34: 25058–25071.
- Chen, J.; Lei, R.; and Wei, Z. 2024. PolyGCL: GRAPH CONTRASTIVE LEARNING via Learnable Spectral Polynomial Filters. In *The Twelfth International Conference on Learning Representations*.
- Childs, L.; Nikoloski, Z.; May, P.; and Walther, D. 2009. Identification and classification of ncRNA molecules using graph properties. *Nucleic acids research*, 37(9): e66–e66.
- Chung, F. R. 1997. *Spectral graph theory*, volume 92. American Mathematical Soc.
- Defferrard, M.; Bresson, X.; and Vandergheynst, P. 2016. Convolutional neural networks on graphs with fast localized spectral filtering. *Advances in neural information processing systems*, 29.
- Ding, K.; Xu, Z.; Tong, H.; and Liu, H. 2022. Data augmentation for deep graph learning: A survey. *ACM SIGKDD Explorations Newsletter*, 24(2): 61–77.
- Dong, X.; Thanou, D.; Toni, L.; Bronstein, M.; and Frossard, P. 2020. Graph signal processing for machine learning: A review and new perspectives. *IEEE Signal processing magazine*, 37(6): 117–127.
- Entezari, N.; Al-Sayouri, S. A.; Darvishzadeh, A.; and Papalexakis, E. E. 2020. All you need is low (rank) defending against adversarial attacks on graphs. In *Proceedings of the 13th International Conference on Web Search and Data Mining*, 169–177.
- Feng, W.; Zhang, J.; Dong, Y.; Han, Y.; Luan, H.; Xu, Q.; Yang, Q.; Kharlamov, E.; and Tang, J. 2020. Graph random neural networks for semi-supervised learning on graphs. *Advances in neural information processing systems*, 33: 22092–22103.
- Feragen, A.; Kasenburg, N.; Petersen, J.; de Bruijne, M.; and Borgwardt, K. 2013. Scalable kernels for graphs with continuous attributes. *Advances in neural information processing systems*, 26.
- Gómez-Bombarelli, R.; Wei, J. N.; Duvenaud, D.; Hernández-Lobato, J. M.; Sánchez-Lengeling, B.; Sheberla, D.; Aguilera-Iparraguirre, J.; Hirzel, T. D.; Adams, R. P.; and Aspuru-Guzik, A. 2018. Automatic chemical design using a data-driven continuous representation of molecules. *ACS central science*, 4(2): 268–276.
- Guo, H.; and Mao, Y. 2021. Intrusion-free graph mixup.
- Hamilton, W.; Ying, Z.; and Leskovec, J. 2017. Inductive representation learning on large graphs. *Advances in neural information processing systems*, 30.
- Hammond, D. K.; Gur, Y.; and Johnson, C. R. 2013. Graph diffusion distance: A difference measure for weighted graphs based on the graph Laplacian exponential kernel. In *2013 IEEE global conference on signal and information processing*, 419–422. IEEE.
- Hammond, D. K.; Vandergheynst, P.; and Gribonval, R. 2011. Wavelets on graphs via spectral graph theory. *Applied and Computational Harmonic Analysis*, 30(2): 129–150.
- Han, X.; Jiang, Z.; Liu, N.; and Hu, X. 2022. G-mixup: Graph data augmentation for graph classification. In *International Conference on Machine Learning*, 8230–8248. PMLR.
- Hassani, K.; and Khasahmadi, A. H. 2020. Contrastive multi-view representation learning on graphs. In *International conference on machine learning*, 4116–4126. PMLR.
- Hu, W.; Fey, M.; Zitnik, M.; Dong, Y.; Ren, H.; Liu, B.; Catasta, M.; and Leskovec, J. 2020a. Open graph benchmark: Datasets for machine learning on graphs. *Advances in neural information processing systems*, 33: 22118–22133.
- Hu, W.; Liu, B.; Gomes, J.; Zitnik, M.; Liang, P.; Pande, V.; and Leskovec, J. 2020b. Strategies for pre-training graph neural networks. In *International Conference on Learning Representations*.
- Jin, G.; Liang, Y.; Fang, Y.; Huang, J.; Zhang, J.; and Zheng, Y. 2023a. Spatio-temporal graph neural networks for predictive learning in urban computing: A survey. *arXiv preprint arXiv:2303.14483*.
- Jin, M.; Shi, G.; Li, Y.-F.; Wen, Q.; Xiong, B.; Zhou, T.; and Pan, S. 2023b. How Expressive are Spectral-Temporal Graph Neural Networks for Time Series Forecasting? *arXiv preprint arXiv:2305.06587*.
- Kipf, T. N.; and Welling, M. 2016a. Semi-supervised classification with graph convolutional networks. *arXiv preprint arXiv:1609.02907*.
- Kipf, T. N.; and Welling, M. 2016b. Variational graph auto-encoders. *arXiv preprint arXiv:1611.07308*.

- Kipf, T. N.; and Welling, M. 2017. Semi-supervised classification with graph convolutional networks. In *In International Conference on Learning Representations*.
- Lee, J. R.; Gharan, S. O.; and Trevisan, L. 2014. Multiway spectral partitioning and higher-order cheeger inequalities. *Journal of the ACM (JACM)*, 61(6): 1–30.
- Lin, L.; Chen, J.; and Wang, H. 2022. Spectral Augmentation for Self-Supervised Learning on Graphs. In *The Eleventh International Conference on Learning Representations*.
- Ling, H.; Jiang, Z.; Liu, M.; Ji, S.; and Zou, N. 2023. Graph Mixup with Soft Alignments. *arXiv preprint arXiv:2306.06788*.
- Liu, N.; Wang, X.; Bo, D.; Shi, C.; and Pei, J. 2022. Revisiting graph contrastive learning from the perspective of graph spectrum. *Advances in Neural Information Processing Systems*, 35: 2972–2983.
- Lutzeyer, J.; and Walden, A. 2017. Comparing graph spectra of adjacency and laplacian matrices. *arXiv preprint arXiv:1712.03769*.
- Ma, H.; Bian, Y.; Rong, Y.; Huang, W.; Xu, T.; Xie, W.; Ye, G.; and Huang, J. 2022. Cross-dependent graph neural networks for molecular property prediction. *Bioinformatics*, 38(7): 2003–2009.
- Morris, C.; Kriege, N. M.; Bause, F.; Kersting, K.; Mutzel, P.; and Neumann, M. 2020. Tudasets: A collection of benchmark datasets for learning with graphs. *arXiv preprint arXiv:2007.08663*.
- Narayanan, A.; Chandramohan, M.; Venkatesan, R.; Chen, L.; Liu, Y.; and Jaiswal, S. 2017. graph2vec: Learning distributed representations of graphs. *arXiv preprint arXiv:1707.05005*.
- Newey, W. K.; and West, K. D. 1987. Hypothesis testing with efficient method of moments estimation. *International Economic Review*, 777–787.
- Newman, M. E.; Watts, D. J.; and Strogatz, S. H. 2002. Random graph models of social networks. *Proceedings of the national academy of sciences*, 99(suppl_1): 2566–2572.
- Nt, H.; and Maehara, T. 2019. Revisiting graph neural networks: All we have is low-pass filters. *arXiv preprint arXiv:1905.09550*.
- Ortega, A.; Frossard, P.; Kovačević, J.; Moura, J. M.; and Vandergheynst, P. 2018. Graph signal processing: Overview, challenges, and applications. *Proceedings of the IEEE*, 106(5): 808–828.
- Park, J.; Shim, H.; and Yang, E. 2022. Graph transplant: Node saliency-guided graph mixup with local structure preservation. In *Proceedings of the AAAI Conference on Artificial Intelligence*, volume 36, 7966–7974.
- Rong, Y.; Huang, W.; Xu, T.; and Huang, J. 2019. DropEdge: Towards Deep Graph Convolutional Networks on Node Classification. In *International Conference on Learning Representations*.
- Sterling, T.; and Irwin, J. J. 2015. ZINC 15–ligand discovery for everyone. *Journal of chemical information and modeling*, 55(11): 2324–2337.
- Sun, F.-Y.; Hoffman, J.; Verma, V.; and Tang, J. 2019. InfoGraph: Unsupervised and Semi-supervised Graph-Level Representation Learning via Mutual Information Maximization. In *ICLR*.
- Suresh, S.; Li, P.; Hao, C.; and Neville, J. 2021. Adversarial graph augmentation to improve graph contrastive learning. *Advances in Neural Information Processing Systems*, 34: 15920–15933.
- Veličković, P.; Fedus, W.; Hamilton, W. L.; Liò, P.; Bengio, Y.; and Hjelm, R. D. 2018. Deep Graph Infomax. In *International Conference on Learning Representations*.
- Verma, V.; Lamb, A.; Beckham, C.; Najafi, A.; Mitliagkas, I.; Lopez-Paz, D.; and Bengio, Y. 2019. Manifold mixup: Better representations by interpolating hidden states. In *International conference on machine learning*, 6438–6447.
- Wang, H.; Zhang, J.; Zhu, Q.; and Huang, W. 2022. Augmentation-free graph contrastive learning with performance guarantee. *arXiv preprint arXiv:2204.04874*.
- Wang, Y.; Wang, W.; Liang, Y.; Cai, Y.; and Hooi, B. 2021. Mixup for node and graph classification. In *Proceedings of the Web Conference 2021*, 3663–3674.
- Wills, P.; and Meyer, F. G. 2020. Metrics for graph comparison: a practitioner’s guide. *Plos one*, 15(2): e0228728.
- Wu, F.; Souza, A.; Zhang, T.; Fifty, C.; Yu, T.; and Weinberger, K. 2019. Simplifying graph convolutional networks. In *International conference on machine learning*, 6861–6871. PMLR.
- Xu, K.; Hu, W.; Leskovec, J.; and Jegelka, S. 2018. How Powerful are Graph Neural Networks? In *International Conference on Learning Representations*.
- Yang, K.; Han, H.; Jin, W.; and Liu, H. 2023. Augment with Care: Enhancing Graph Contrastive Learning with Selective Spectrum Perturbation. *arXiv preprint arXiv:2310.13845*.
- Yang, M.; Shen, Y.; Li, R.; Qi, H.; Zhang, Q.; and Yin, B. 2022. A new perspective on the effects of spectrum in graph neural networks. In *International Conference on Machine Learning*, 25261–25279. PMLR.
- Yi, H.-C.; You, Z.-H.; Huang, D.-S.; and Kwok, C. K. 2022. Graph representation learning in bioinformatics: trends, methods and applications. *Briefings in Bioinformatics*, 23(1): bbab340.
- Yoo, J.; Shim, S.; and Kang, U. 2022. Model-agnostic augmentation for accurate graph classification. In *Proceedings of the ACM Web Conference 2022*, 1281–1291.
- You, Y.; Chen, T.; Shen, Y.; and Wang, Z. 2021. Graph contrastive learning automated. In *International Conference on Machine Learning*, 12121–12132. PMLR.
- You, Y.; Chen, T.; Sui, Y.; Chen, T.; Wang, Z.; and Shen, Y. 2020. Graph contrastive learning with augmentations. *Advances in neural information processing systems*.
- Zhang, H.; Cisse, M.; Dauphin, Y. N.; and Lopez-Paz, D. 2017. mixup: Beyond empirical risk minimization. *arXiv preprint arXiv:1710.09412*.
- Zhao, T.; Jin, W.; Liu, Y.; Wang, Y.; Liu, G.; Günnemann, S.; Shah, N.; and Jiang, M. 2022. Graph data augmentation for graph machine learning: A survey. *arXiv preprint arXiv:2202.08871*.

Appendix

Details of Datasets

We conduct our experiments on 21 different graph real-world datasets for graph classification tasks. In this section, we provide detailed descriptions of the datasets used in this paper. Specifically, for the *supervised* learning setting, we include a total of eight datasets from the TUDatasets benchmark (Morris et al. 2020) (i.e., PROTEINS, NCI1, IMDB-BINARY, IMDB-MULTI, REDDIT-BINARY, REDDIT-MULTI-5K, and REDDIT-MULTI-12K) and the OGB benchmark (Hu et al. 2020a) (i.e., ogbg-molhiv). For the *semi-supervised* learning setting, we include seven different datasets from the TUDatasets benchmark (Morris et al. 2020) (i.e., PROTEINS, NCI1, DD, COLLAB, GITHUB, REDDIT-BINARY, and REDDIT-MULTI-5K). For the *unsupervised* learning setting, we include seven different datasets from the TUDatasets benchmark (Morris et al. 2020) (i.e., PROTEINS, NCI1, DD, MUTAG, IMDB-BINARY, REDDIT-BINARY, and REDDIT-MULTI-5K). The detailed of these datasets can be found in Table 5.

For the *transfer* learning setting, we pre-train on ZINC-2M chemical molecule dataset (Sterling and Irwin 2015; Gómez-Bombarelli et al. 2018), and fine-tune on eight different datasets, namely BBBP, Tox21, ToxCast, SIDER, ClinTox, MUV, HIV, and BACE. The detailed of these datasets can be found in Table 6.

Table 6: Statistical characteristics of the datasets used in the transfer learning setting.

Dataset	Strategy	# Molecules	# Binary tasks
ZINC-2M	Pre-training	2,000,000	-
BBBP	Fine-tuning	2,039	1
Tox21	Fine-tuning	7,831	12
ToxCast	Fine-tuning	8,576	617
SIDER	Fine-tuning	1,427	27
ClinTox	Fine-tuning	1,477	2
MUV	Fine-tuning	93,087	17
HIV	Fine-tuning	41,127	1
BACE	Fine-tuning	1,513	1

Details of Baselines

Supervised learning. For experiments in the supervised setting, we select the following baseline:

- DropEdge (Rong et al. 2019) selectively drops a portion of edges from the input graphs.
- DropNode (Feng et al. 2020) omits a specific ratio of nodes from the provided graphs.
- Subgraph (You et al. 2020) procures subgraphs from the main graphs using a random walk sampling technique.
- M-Mixup (Verma et al. 2019) blends graph-level representations through linear interpolation.
- SubMix (Yoo, Shim, and Kang 2022) combines random subgraphs from paired input graphs.
- G-Mixup (Han et al. 2022) employs a class-focused graph mixup strategy by amalgamating graphons across various classes.

- S-Mixup (Ling et al. 2023) adopts a mixup approach for graph classification, emphasizing soft alignments.

Semi-supervised learning. For experiments in the semi-supervised setting, we select the following baseline methods:

- GAE (Kipf and Welling 2016b) is a non-probabilistic graph auto-encoder model, which is a variant of the VGAE (variational graph autoencoder).
- Informax (Veličković et al. 2018) trains a node encoder to optimize the mutual information between individual node representations and a comprehensive global graph representation.
- GraphCL (You et al. 2020) conducts an in-depth exploration of graph structure augmentations, including random edge removal, node dropping, and subgraph sampling.

Unsupervised learning. For experiments in the unsupervised setting, we select the following baseline methods:

- sub2vec (Adhikari et al. 2018) seeks to capture feature representations of arbitrary subgraphs, addressing the limitations of node-centric embeddings.
 - graph2vec (Narayanan et al. 2017) is a neural embedding framework designed to learn data-driven distributed representations of entire graphs.
 - InfoGraph (Sun et al. 2019) is designed to maximize the mutual information between complete graph representations and various substructures, such as nodes, edges, and triangles.
 - GraphCL (see above section).
 - MVGRL (Hassani and Khasahmadi 2020) establishes a link between the local Laplacian matrix and a broader diffusion matrix by leveraging mutual information. This approach yields representations at both the node and graph levels, catering to distinct prediction tasks.
 - AD-GCL (Suresh et al. 2021) emphasize preventing the capture of redundant information during training. They achieve this by optimizing adversarial graph augmentation strategies in GCL and introducing a trainable non-i.i.d. edge-dropping graph augmentation.
 - JOAO (You et al. 2021) utilize a bi-level optimization framework to sift through optimal strategies, exploring multiple augmentation types like uniform edge or node dropping and subgraph sampling.
 - GCL-SPAN (Lin, Chen, and Wang 2022) introduces a spectral augmentation approach, which directs topology augmentations to maximize spectral shifts.
- Transfer learning.** For experiments in the transfer setting, we select the following baseline methods:
- Informax (see above section).
 - EdgePred (Hamilton, Ying, and Leskovec 2017) employs an inductive approach that utilizes node features, such as text attributes, to produce node embeddings by aggregating features from a node’s local neighborhood, rather than training distinct embeddings for each node.

Table 5: Statistical characteristics of the datasets in three learning settings. Supe.: Supervised learning. Semi.: Semi-supervised learning. Unsu.: Unsupervised learning.

Dataset	Category	# Graphs	# Avg edges	# Classes	Task		
					Supe.	Semi.	Unsu.
IMDB-BINARY	Social Networks	1,000	96.53	2	✓		✓
IMDB-MULTI	Social Networks	1,500	65.94	3	✓		
REDDIT-BINARY	Social Networks	2,000	497.75	2	✓	✓	✓
REDDIT-MULTI-5K	Social Networks	4,999	594.87	5	✓	✓	✓
REDDIT-MULTI-12K	Social Networks	11,929	456.89	11	✓		
COLLAB	Social Networks	5,000	2457.78	3		✓	
GITHUB	Social Networks	12,725	234.64	2		✓	
DD	Biochemical Molecules	1,178	715.66	2		✓	✓
MUTAG	Biochemical Molecules	188	19.79	2			✓
PROTEINS	Biochemical Molecules	1,113	72.82	2	✓	✓	✓
NCII	Biochemical Molecules	4,110	32.30	2	✓	✓	✓
ogbg-molhiv	Biochemical Molecules	41,127	27.50	2	✓		

- AttrMasking (Attribute Masking) (Hu et al. 2020b) is a pre-training method for GNNs that harnesses domain knowledge by discerning patterns in node or edge attributes across graph structures.
- ContextPred (Context Prediction) (Hu et al. 2020b) is designed for pre-training GNNs that simultaneously learn local node-level and global graph-level representations via subgraphs to predict their surrounding graph structures.
- GraphCL (see above section).

Details of Experiments Settings

We conduct our experiments with PyTorch 1.13.1 on a server with NVIDIA RTX A5000 and CUDA 12.2. For each experiment, we run 10 times. We detail the settings of our experiments in this paper as follows.

Speed up implementation. Our augmentation method involves matrix eigenvalue decomposition, which is highly CPU-intensive. During implementation, we observed that when there is insufficient CPU, parallelly executing numerous matrix eigenvalue decomposition can lead to CPU resource deadlock. To address this issue, we established an additional set of CPU locks to manage CPU scheduling. Let N_{cpu} represent the number of CPUs available for each matrix eigenvalue decomposition task, and $N_{parallel}$ denote the number of decomposition tasks that can be executed simultaneously. We set $N_{cpu} \times N_{parallel}$ to be less than the total CPU number of the server. During task execution, we created a list of CPU locks, with each lock corresponding to N_{cpu} available CPUs. There is no overlap between the CPUs corresponding to each lock. Before a matrix decomposition task is executed, it must first request a CPU lock. Once the lock is acquired, the task can only be executed on the designated CPUs. After completion, the task releases the CPU lock. If there are no free locks in the current CPU lock list, the matrix decomposition task must wait. By employing this approach, we effectively isolated parallel matrix decomposition tasks.

Empirical studies. We first detail the processes and settings of the empirical studies below.

- **Experiment of Figure 1.** For DropEdge, 20% edges are randomly dropped. For DP-Noise, we use a standard de-

viation of 7, an augmentation probability of 0.5, and an augmentation frequency ratio of 0.5. For DP-Mask, the augmentation probability is set to 0.3, with an augmentation frequency ratio of 0.4. Detailed variations in edge numbers and properties between the original and augmented graphs can be found in Table 7.

- **Experiment of Figure 4.** In Figures 4a and 4b, labels in REDDIT-MULTI-12K for Class A and Class B are 1 and 10, respectively. The added edges in 4c are $3 \leftrightarrow 5$, $3 \leftrightarrow 7$, $1 \leftrightarrow 6$, $2 \leftrightarrow 6$, $0 \leftrightarrow 2$, $1 \leftrightarrow 3$, $1 \leftrightarrow 4$, $2 \leftrightarrow 4$, $4 \leftrightarrow 6$, and $5 \leftrightarrow 7$, respectively. The dropped edges in 4d are $0 \leftrightarrow 4$, $3 \leftrightarrow 4$, $4 \leftrightarrow 5$, $4 \leftrightarrow 7$, $0 \leftrightarrow 1$, $2 \leftrightarrow 3$, $0 \leftrightarrow 3$, $5 \leftrightarrow 6$, $6 \leftrightarrow 7$, and $1 \leftrightarrow 2$, respectively. The change of spectrum ΔL_2 is the L_2 distance between the spectrum of \mathcal{G} and augmented graph \mathcal{G}' , denoted as $\Delta L_2 = \sqrt{\sum_i (\lambda_i(\mathcal{G}) - \lambda_i(\hat{\mathcal{G}}))^2}$, where $\lambda(\mathcal{G})$ represent the spectrum of \mathcal{G} and $\lambda(\hat{\mathcal{G}})$ is the spectrum of $\hat{\mathcal{G}}$.
- **Experiment of Figure 3.** For both Figure 3a and 3b, we employ GIN as the backbone model and conduct experiments over five runs. In Figure 3b, while testing one parameter, we draw the other parameters from their respective search spaces: $\sigma \in [0.1, 0.5, 1.0, 2.0]$, $r_f \in [0.1, 0.2, 0.3, 0.4, 0.5, 0.6, 0.7, 0.8]$, and $r_a \in [0, 0.2, 0.4, 0.6, 0.8, 1]$. In addition, to control the noise adding to low- and high-frequency eigenvalues are in the same scale, the augmented i -th eigenvalue is calculated as $\lambda_i = \max(0, 1 + \epsilon) \times \lambda_i$, where $\epsilon \sim \mathcal{N}(0, \sigma)$.

Supervised learning. Following prior works (Han et al. 2022; Ling et al. 2023), we utilize two GNN models, namely GCN (Kipf and Welling 2017) and GIN (Xu et al. 2018). Details of these GNNs are provided below.

- **GCN.** For the TUDatasets benchmark, the backbone model has four GCN layers, utilizes a global mean pooling readout function, has a hidden size of 32, and uses the ReLU activation function. For the ogbg-molhiv dataset, the model consists of five GCN layers, a hidden size of 300, the ReLU activation function, and a global mean pooling readout function.
- **GIN.** For the TUDatasets benchmark, the backbone model comprises four GIN layers, each with a two-layer

Table 7: Details of alterations of the number of edges and properties of graphs in Figure 1.

Graph	Edge Alterations		Properties				
	# Dropped	# Added	Connectivity	Diameter	Radius	# Periphery	ASPL
Original	-	-	TRUE	2	1	11	1.42
DropEdge	7	0	TRUE	3	2	8	1.64
DP-Noise	6	0	TRUE	2	1	11	1.52
DP-Mask	14	4	TRUE	2	1	11	1.58

MLP. It utilizes a global mean pooling readout function, has a hidden size of 32, and adopts the ReLU activation function. Conversely, for the ogbg-molhiv dataset, the model consists of five GIN layers, a hidden size of 300, the ReLU activation function, and employs a global mean pooling for the readout function.

For all other hyper-parameter search space and training configurations of the experiments on the IMDB-B, IMDB-M, REDD-B, REDD-M5, and REDD-M12, we keep consistent with (Han et al. 2022). For all other hyper-parameter search space and training configurations of the experiments on the PROTEIN, NCI1, and ogbg-hiv, we keep consistent with (Ling et al. 2023). Note that instead of adopting the results of baseline methods on the ogbg-hiv dataset from the reference directly, we reported the results of rerunning the baseline experiments on the ogbg-hiv dataset, which is higher than the results in the reference.

Semi-supervised learning. We maintain consistency with (You et al. 2020) for all hyper-parameter search spaces and training configurations. For all datasets, we conduct experiments at label rates of 1% (provided there are more than 10 samples for each class) and 10%. These experiments are performed five times, with each instance corresponding to a 10-fold evaluation. We report both the mean and standard deviation of the accuracies in percentages. During pre-training, we perform a grid search, tuning the learning rate among 0.01, 0.001, 0.0001 and the epoch number within 20, 40, 60, 80, 100.

Unsupervised representation learning. Following (You et al. 2020; Lin, Chen, and Wang 2022), we use a 5-layer GIN as encoders. For all hyper-parameter search spaces and training settings in unsupervised learning, we also align with the configurations presented in (You et al. 2020). We conduct experiments five times, with each iteration corresponding to a 10-fold evaluation. The reported results in Table 4 include both the mean and standard deviation of the accuracy percentages.

Transfer learning. Following the transfer learning setting in (Hu et al. 2020b; You et al. 2020; Lin, Chen, and Wang 2022), we conduct graph classification experiments on a set of biological and chemical datasets via GIN models. Specifically, an encoder was first pre-trained on the large ZINC-2M chemical molecule dataset (Sterling and Irwin 2015; Gómez-Bombarelli et al. 2018) and then was evaluated on small datasets from the same domains (i.e., BBBP, Tox21, ToxCast, SIDER, ClinTox, MUV, HIV, and BACE).

More Experiments Results

Transfer learning. We draw comparisons between our methods and six baselines, including a reference model

without pre-training (referred to *No-Pre-Train*), Informax (Veličković et al. 2018), EdgePred (Hamilton, Ying, and Leskovec 2017), AttrMasking (Hu et al. 2020b), ContextPred (Hu et al. 2020b) and GraphCL (You et al. 2020). The comparative results are shown in Table 8. Our methods demonstrated SOTA performance, outperforming competitors on half of the datasets. Especially, our methods consistently outperform the conventional GraphCL method, which indicates our data augmentation methods as better choices for graph contrastive learning. Notably, DP-Mask achieves an 83.52% ROC-AUC score on ClinTox, exceeding the performance of GraphCL by a substantial margin (nearly 10%). These findings demonstrate the enhanced efficacy of our techniques in the transfer learning setting for graph classification tasks.

Empirical studies. In Section , we investigate spectral alterations due to adding an edge in a toy graph (depicted in Figure 2a). The spectral changes are presented in Figure 2b. Further, in Figure 7, we analyze the consequences on the spectrum when edges from the same toy graph are removed. Notably, the removal of edges 0-4 and 3-4 results in minimal spectral variations. However, the removal of edges 5-6 and 6-7 leads to pronounced changes in both high and low frequencies, evident from the pronounced shifts in values λ_2 and λ_5 . To further illustrate our observation, we present an additional example featuring a nine-node toy graph that also exhibits similar results, as shown in Figure 8.

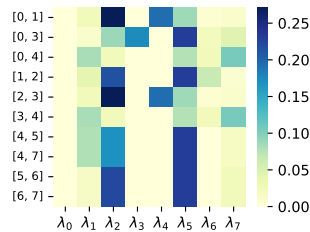


Figure 7: Absolute variation of eigenvalues when dropping different edges of the toy graph.

Hyperparameter sensitivities. We conducted experiments on the IMDB-BINARY dataset, leveraging various combinations of standard deviation σ and frequency ratio r_f for both low and high-frequency components to assess the impacts of DP-Noise parameters. For these experiments, we employed the GIN as our backbone model let σ and r_f from two search spaces, where $\sigma \in [0.1, 0.5, 1.0, 2.0]$ and $r_f \in [0.1, 0.2, 0.3, 0.4, 0.5, 0.6, 0.7, 0.8]$. We run 5 experiments and report the average values in Figure 9. Our observations indicate that introducing noise in the high-

Table 8: Performance comparisons in the *transfer learning* setting. The best and second best results are highlighted with **bold** and underline, respectively. The metric is ROC-AUC scores (%). * and ** denote the improvement over the second-best baseline is statistically significant at levels 0.1 and 0.05, respectively. Baseline results are taken from (Hu et al. 2020b; You et al. 2020).

Dataset	BBBP	Tox21	ToxCast	SIDER	ClinTox	MUV	HIV	BACE
No-Pre-Train	65.80± 4.50	74.00± 0.80	63.40± 0.60	57.30± 1.60	58.00± 4.40	71.80± 2.50	75.30± 1.90	70.10± 5.40
Infomax	68.80± 0.80	75.30± 0.50	62.70± 0.40	58.40± 0.80	69.90± 3.00	<u>75.30± 2.50</u>	76.00± 0.70	75.90± 1.60
EdgePred	67.30± 2.40	76.00± 0.60	64.10± 0.60	60.40± 0.70	64.10± 3.70	74.10± 2.10	76.30± 1.00	79.90± 0.90
AttrMasking	64.30± 2.80	76.70± 0.40	64.20± 0.50	61.00± 0.70	71.80± 4.10	74.70± 1.40	77.20± 1.10	79.30± 1.60
ContextPred	68.00± 2.00	75.70± 0.70	63.90± 0.60	60.90± 0.60	65.90± 3.80	75.80± 1.70	77.30± 1.00	79.60± 1.20
GraphCL	69.68± 0.67	73.87± 0.66	62.40± 0.57	60.53± 0.88	75.99± 2.65	69.80± 2.66	78.47± 1.22	75.38± 1.44
DP-Noise	70.38± 0.91*	74.33± 0.42	64.08± 0.25	61.52± 0.79	76.26± 1.68	74.09± 2.30	78.63± 0.37	77.37± 1.76
DP-Mask	71.63± 1.86**	75.51± 0.26	63.77± 0.22	61.33± 0.17	83.52± 1.07**	75.02± 0.36	78.73± 0.77	79.45± 0.69

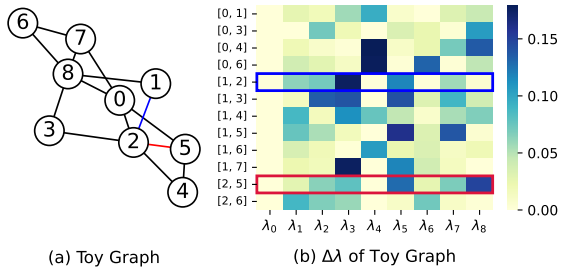


Figure 8: (a) Another toy graph \mathcal{G}' consisting of nine nodes. (b) Absolute variation in eigenvalues of \mathcal{G}' when adding an edge at diverse positions. The red and blue rectangles represent when adding the corresponding edges in \mathcal{G}' and the change of the eigenvalues.

frequency components tends to enhance the test accuracy more markedly than when infused in the low-frequency regions, as illustrated by the prevailing lighter color in Figure 9a. This observation resonates with the insights gleaned from Section . Building upon these general observations, we further elucidate the effects of each specific parameter below.

- **Effects of Standard Deviation σ .** For low-frequency components, the introduction of noise seems to not exhibit a consistent influence on accuracy. In contrast, when noise is applied to high-frequency components, we observe a discernible trend: accuracy tends to increase with increasing standard deviations. This suggests that the diversity introduced by elevating the standard deviation of noise can potentially bolster the classification performance of generated graphs.
- **Effects of Frequency Ratio r_f .** Similar to σ , for low-frequency components, increasing r_f does not consistently enhance or degrade accuracy across different standard deviations. On the other hand, in the high-frequency regime, a subtle trend emerges. As r_f increases, there is a nuanced shift in accuracy, suggesting that the spectrum of frequencies impacted by the noise has a nuanced interplay with the graph’s inherent structures and the subsequent classification performance.

We also conduct hyperparameter analysis in different learning settings. Figure 10 shows performances across

multiple datasets, which reveals distinct trends in performance related to augmentation probability (*aug_prob*) and frequency ratio (*aug_freq_ratio*). Specifically, for the DD dataset, performance peaks with a high *aug_freq_ratio* and *aug_prob*, suggesting a preference for more frequent augmentations. In contrast, the MUTAG dataset shows optimal results at a lower frequency but higher probability, indicating a different augmentation response. The NC11 dataset’s best performance occurs at higher values of both parameters, while REDDIT-BINARY favors moderate to high frequency combined with a high probability, achieving its peak performance under these conditions. These patterns highlight the necessity of customizing hyperparameters to each dataset for optimal augmentation effectiveness.

Complexity and Time Analysis. Theoretically, the computational bottleneck of our data augmentation method primarily stems from the eigen-decomposition and reconstruction of the Laplacian matrix. For a graph with n nodes, the computational complexity of both operations is $O(n^3)$. In terms of implementation, we have measured the time cost required by our method. For each n , we randomly generated 100 graphs and recorded the average time and standard deviation required for our data augmentation method. The results, presented in Table 9, are measured in milliseconds. The average number of nodes in commonly used graph classification datasets is approximately between 10 and 500. Therefore, in the majority of practical training scenarios, the average time consumption of our algorithm for augmenting a single graph is roughly between 1 millisecond and 40 milliseconds. The experiments conducted here did not employ any parallel computing or acceleration methods. However, in actual training processes, it is common to parallelize data preprocessing using multiple workers or to precompute and store the eigen-decomposition results of training data. Therefore, the actual time consumption required for our method in implementations will be even lower. Therefore, **although the complexity is theoretically high, in fact, the time required is practically low.**

More Discussions

Advantages of the proposed method. At the heart of data augmentation lies a dual objective: to preserve the essence of the data while expanding its diversity. Our approach strikes this balance skillfully. Leveraging spectral view, it safeguards key graph property (Figure 1e), ensuring the aug-

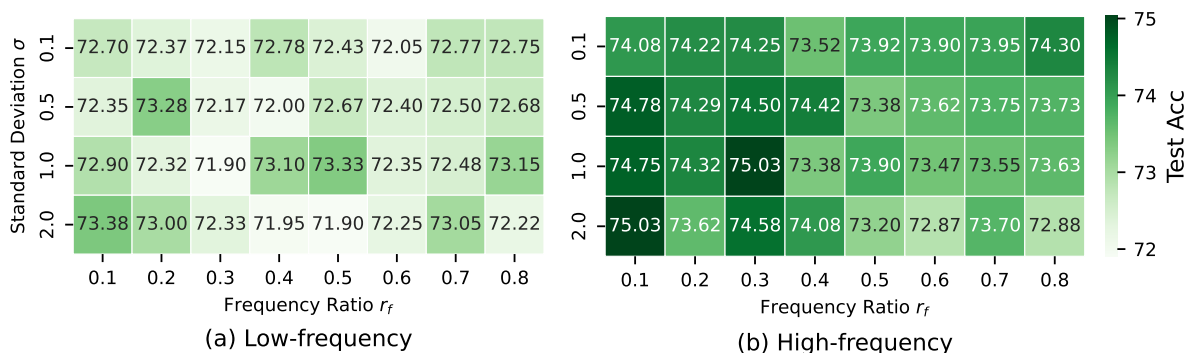


Figure 9: Effects of different hyperparameter combinations on the IMDB-BINARY dataset in the supervised learning setting for graph classification via adding noise to (a) low-frequency and (b) high-frequency eigenvalues, respectively. The evaluation metric is accuracy.

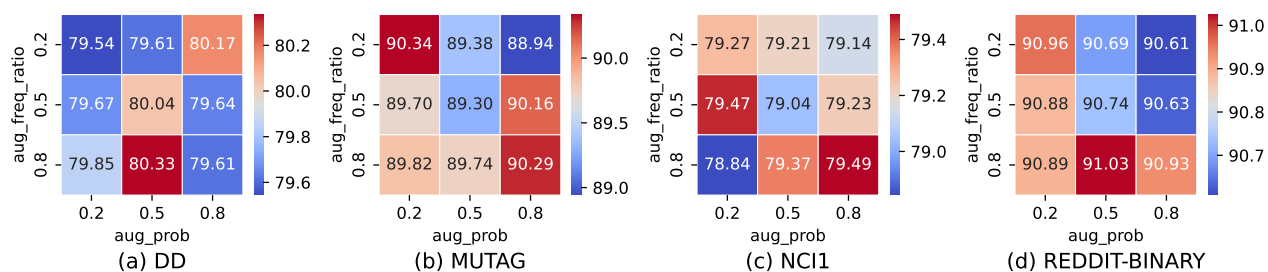


Figure 10: Effects of different hyperparameter combinations on different datasets in the unsupervised learning setting for graph classification via masking. The evaluation metric is accuracy.

mented data remains authentic and relevant. This not only enhances the training data’s quality but also directly boosts the performance, as detailed in the following section.

Comparison with existing works. Our method distinguishes itself from three related spectral view works: (Liu et al. 2022), (Lin, Chen, and Wang 2022), and (Yang et al. 2023). (Liu et al. 2022) focuses on optimal contrastive pair selection instead of a general augmentation method, and GCL-SPAN (Lin, Chen, and Wang 2022) centers on maximizing spectral variance. However, our observations suggest that broad spectral changes do not always correspond with graph properties. In addition, though GCL-SPAN also use a spectral perspective, it essentially alters the spatial domain, instead of direct spectral modifications, while our method’s enhanced performance underlines the effectiveness of spectral alterations. GASSER (Yang et al. 2023) perturbs different frequency bands to uphold homophily ratios and fine-tune task-specific features. Whereas our approach concentrates on the essential structural integrity required for graph classification.

Broader Impact. Through a spectral lens, our proposed augmentation method presents both significant advancements and implications in the realm of graph-based learning. This can lead to improved performance, robustness, and generalizability of graph neural networks (GNNs) across a myriad of applications, from social network analysis to molecu-

lar biology. In addition, by utilizing spectral properties, our method provides a more transparent approach to augmentation. This can help researchers and practitioners better understand how alterations to graph structures impact learning outcomes, thereby aiding in the interpretability of graph data augmentation. While there is a superficial overlap in terms of using “spectrum” for “graph data augmentation” with some related works, e.g., (Liu et al. 2022; Lin, Chen, and Wang 2022), the core methodologies and outcomes are distinctly different. *We believe it should be a new direction and open up new avenues for spectral-based augmentation techniques, allowing more diverse research on doing the augmentation on the spectrum.*

Limitations & Future Directions. A potential limitation of this study is its primary emphasis on homophily graphs. In contrast, heterophily graphs, where high-frequency information plays a more crucial role, are not extensively addressed (Bo et al. 2021). In addition, as we have discussed on the characteristics of molecular datasets above, in some situations, the high-frequency component may also include important information for graph classification tasks. Looking ahead, it would be worth investigating learning strategies tailored to selectively alter eigenvalues, ensuring adaptability across diverse datasets. This includes developing methods to safely create realistic augmented graphs and experimenting with mix-up techniques involving eigenvalues from different

Table 9: Time cost required by our method. n : Number of nodes.

	$n = 10$	$n = 20$	$n = 100$	$n = 200$	$n = 500$	$n = 1000$
Time(ms)	0.76 ± 0.55	0.89 ± 0.43	2.50 ± 0.50	6.45 ± 0.58	41.35 ± 2.39	230.75 ± 8.76

graphs.

High-Frequency Significance in Molecular Data. Incorporating insights from Table 8, our method shows varied performance across datasets. Specifically, within the Tox21 and ToxCast toxicology datasets, our approach does not achieve top-ranking results. This could be due to the potential significance of high-frequency components in capturing essential structural details within these datasets, which aligns with the intricate biological nature of the targets and stress response pathways represented in these datasets. The Tox21 dataset contains qualitative toxicity measurements for various biological targets, such as nuclear receptors and stress response pathways (Ma et al. 2022), which could be notably influenced by subtle molecular changes detected in the high-frequency domain. Consequently, it is plausible to suggest that high-frequency components play a vital role in distinguishing between toxic and non-toxic molecules by capturing subtle molecular differences crucial for predicting bioactivity and toxicity. In contrast to datasets focusing on broader properties like BBBP (Blood-Brain Barrier permeability) or BACE (inhibitor activity against beta-secretase), Tox21 and ToxCast encompass a wide range of bioassays that may be particularly sensitive to the high-frequency intricacies of molecular structures. Thus, the complexity of molecular compositions and the diversity of bioactivity assays in Tox21 and ToxCast imply that high-frequency components may contain essential information for toxicity prediction that may not be as pronounced in datasets such as BBBP.

Rationale for Choosing Graph Laplacian Decomposition. In our methodology, we chose to decompose the graph Laplacian L (where $L = D - A$) to do the perturbation and then reconstruct the graph. In terms of implementation, an alternative method can be directly decomposing A and perturbing its smaller eigenvalues. However, our motivation for this work is more on the inherent properties of graphs, and L offers a more nuanced reflection of these properties compared to A (Lutzeyer and Walden 2017). For future scenarios involving more complex disturbances to eigenvalues, leveraging the eigenvalues of L would be a more appropriate approach. In addition, our decision to decompose L also follows general spectral graph convolution methodologies (Kipf and Welling 2016a).

Loss-pass Filtering of GNNs vs. DP Augmentation. We then discuss the relationships and differences between the loss-pass filtering of GNNs, caused by the model’s neighborhood aggregation processes (Nt and Machara 2019; Kipf and Welling 2017), and our proposed methods.

- *Relationship.* The low-pass effect of GNNs exactly aligns with our motivation - increasing the diversity of data (i.e. altering the high-frequency part) without misguiding the classification (i.e. preserving the low-frequency part). In other words, because DP augmentation enhances the

training-data diversity by introducing randomness to the high-frequency spectrum, the low-pass effect of GNNs preserves the core attributes necessary for correct classification, ensuring label consistency across original and augmented data. By using this natural smoothing capability, our method introduces label-consistent variations to the data. This strategy boosts model robustness and generalization without compromising classification accuracy, affirming the efficacy and theoretical integrity of our method.

- *Difference.* From the signal processing perspective, our method is more like introducing random perturbations to high-frequency components rather than acting as another low-pass filter. For better intuitive understanding, take the image processing as an example, a low-pass filter achieves image denoising, while random perturbation of high-frequency noise sharpens images. These two effects are different and even have a certain degree of opposition. Due to such difference, these two operations can be used jointly during the image processing - in our work, we first use augmentation to randomly perturb the high-frequency part, and then pass it through the low pass filter of GNNs.

Possible reasons of why DP-Noise outperforms DP-Mask. DP-Noise applies subtle, controlled noise to high-frequency eigenvalues, preserving essential low-frequency components while introducing diversity through minor spectral changes. This balance allows DP-Noise to produce augmented graphs that are both diverse and stable, enhancing model generalization and robustness. Conversely, DP-Mask removes selected high-frequency eigenvalues outright, creating more pronounced structural shifts. While effective in diversifying, this approach can introduce instability by over-modifying spectral components, impacting performance consistency.